A Versatile Setup for Fourier-Transform Infrared Magneto-Spectroscopy

Jana Dubnická Midlíková, Matúš Šedivý, Antonín Sojka, Vinicius Tadeu Santana, Adam Dubroka, and Petr Neugebauer

***Abstract*— Fourier-transform infrared (FTIR) magneto-spectroscopy is a powerful spectroscopic technique used to investigate many important effects in materials, e.g., electron spin resonance (ESR), cyclotron resonance, and transitions between Landau levels (LLs). Despite their enormous potential in material science, infrared (IR) magneto-spectrometers are still relatively rare and custom-made since such systems generally require complex infrastructure. This article presents a versatile broadband setup for FTIR magneto-spectroscopy spanning the range from THz/far-IR (FIR) to near-IR (NIR), high magnetic field up to 16 T, and cryogenic temperatures down to 2 K. It consists of a commercial FTIR spectrometer and 16 T cryogen-free superconducting magnet coupled with custom-designed optical coupling and transmission probes for experiments with various detectors. The functionality of the FTIR magneto-spectroscopic setup is demonstrated by the magneto-optical measurements on a cobalt-based single-molecule magnet (SMM) in the FIR region and germanium (Ge) in the NIR region.**

***Index Terms*— Cryogen-free superconducting magnet, electron spin resonance (ESR), Fourier-transform infrared (FTIR) magneto-spectroscopy, germanium (Ge), Landau levels (LLs), single-molecule magnets (SMMs).**

Manuscript received 3 February 2023; revised 15 May 2023; accepted 29 May 2023. Date of publication 9 June 2023; date of current version 29 June 2023. This work was supported by the Ministry of Education, Youth and Sports (MEYS) of the Czech Republic (CR) at Central European Institute of Technology (CEITEC) Nano Research Infrastructure through the CzechNanoLab under Project LM2023051. The work of Jana Dubnická Midlíková was supported in part by the MEYS CR under the INTER-EXCELLENCE Program under Grant LTAUSA19060; and in part by the Brno Ph.D. Talent 2018 Scholarship by South Moravian Centre for International Mobility (JCMM). The work of Antonín Sojka was supported by the MEYS CR under the INTER-EXCELLENCE Program under Grant LTAUSA19060. The work of Matúš Šedivý was supported by the European Research Council (ERC) through the European Union's Horizon 2020 Research and Innovation Program under Grant 714850 and in part by the Brno University of Technology Internal Grant Agency Project under Grant FEKT-S-20-6215. The work of Vinicius Tadeu Santana was supported by the Czech Science Foundation (GACR) under Grant GA23-05578S. The work of Adam Dubroka was supported by the GACR under Project GA20-10377S. The work of Petr Neugebauer was supported by the GACR under Grant EXPRO: 21-20716X. The Associate Editor coordinating the review process was Dr. Jae-Ho Han. *(Corresponding author: Petr Neugebauer.)*

Jana Dubnická Midlíková, Matúš Šedivý, Antonín Sojka, Vinicius Tadeu Santana, and Petr Neugebauer are with the Central European Institute of Technology (CEITEC), Brno University of Technology, 61200 Brno, Czech Republic (e-mail: jana.midlikova@ceitec.vutbr.cz; petr.neugebauer@ceitec.vutbr.cz).

Antonin Sojka was with the Central European Institute of Technology (CEITEC), Brno University of Technology, 61200 Brno, Czech Republic. He is now with the University of California, Santa Barbara, Santa Barbara, CA 93106, USA.

Adam Dubroka is with the Central European Institute of Technology, Brno University of Technology, 61200 Brno, Czech Republic, and also with the Department of Condensed Matter Physics, Faculty of Science, Masaryk University, 61137 Brno, Czech Republic.

This article has supplementary downloadable material available at https://doi.org/10.1109/TIM.2023.3284943, provided by the authors.

Digital Object Identifier 10.1109/TIM.2023.3284943

I. Introduction

INFRARED (IR) spectroscopy is considered one of the most powerful and widespread spectroscopic tools of the 20th and 21st centuries [1]. It provides detailed information about molecular vibrations, which are useful for identifying molecules, studying their structure, and interactions with a surrounding environment [1]. A major breakthrough in IR spectroscopy that led to its widespread use came in the 1970s with the introduction of Fourier-transform IR (FTIR) spectrometers equipped with interferometers, exploiting the well-established mathematical process of Fourier transform (FT) [2]. Due to its significantly improved acquisition of IR spectra, leading to better signal-to-noise and reduced data acquisition time, the FTIR spectrometers are nowadays predominantly used spectrometers in the IR range [3]. Thus, IR spectroscopy is frequently referred to as FTIR spectroscopy. The IR region, roughly defined in the range 10–12 500 cm^{-1} (1 mm–800 nm, 1.24 meV–1.56 eV, 300 GHz–375 THz), is rather broad in terms of energy; therefore, it is divided into three regions: near-IR (NIR) (4000–12 500 cm^{-1}), mid-IR (MIR) (400–4000 cm^{-1}), and far-IR (FIR) (10–400 cm^{-1}) [4]. For the last two decades, THz spectroscopy has developed remarkably due to its intriguing applications in solid-state physics, material science, etc., [5], [6]. The THz region is usually defined as the region extending from 0.1 to 3 THz (3.3–100 cm^{-1}), filling the frequency gap between the microwaves (MWs) and the IR region [7].

The presence of a magnetic field expands the range of phenomena observable by FTIR spectroscopy to, e.g., electron spin resonance (ESR), cyclotron resonance, and transitions between Landau levels (LLs) [8], [9]. FTIR spectroscopy in high magnetic fields hereinafter referred to as FTIR magneto-spectroscopy, especially in low temperatures, is an ideal spectroscopic technique to study new physical phenomena and elucidate the exotic behavior of novel materials, such as single-molecule magnets (SMMs) [10], [11], [12], [13], [14], [15], [16], [17], [18], graphene [19], [20], [21], [22], [23], topological insulators [24], [25], [26], Weyl semimetals [27], [28], or superconductors [29], [30].

High magnetic fields are commonly achieved using superconducting magnets cooled by liquid helium (LHe). Operating and maintaining these magnets in laboratories requires a dedicated infrastructure (helium recovery system, liquefiers) and periodic transfer of cryogenic fluids. Nonetheless, with the development of cryogen-free superconducting magnets in recent years [31], [32], [33], experiments in high magnetic fields have become feasible also for facilities without

LHe infrastructure. Cryogen-free superconducting magnets are becoming popular due to their relatively simple operation compared to conventional LHe-cooled superconducting magnets [31].

Several different experimental configurations utilizing FTIR magneto-spectroscopy are available worldwide. Such systems are frequently an integral part of large research facilities for high magnetic fields, such as the Grenoble High Magnetic Field Laboratory (GHMFL) in France [12] or the National High Magnetic Field Laboratory (NHMFL) in Tallahassee, Florida, USA [18]. Some research facilities utilize synchrotrons as a source of radiation to improve the performance in the FIR and THz regions, e.g., Helmholtz Zentrum Berlin (HZB) operating the BESSY II synchrotron [34], [35], or IR beamline U12IR at the National Synchrotron Light Source (NSLS) of Brookhaven National Laboratory [36]. However, IR magneto-spectroscopic setups can also be found at a few university laboratories/research centers [8], [23], [37], [38], [39], [40], [41], [42], [43].

In this article, we describe the design and implementation of a versatile broadband FTIR magneto-spectroscopic set up in the range 50–10 000 cm^{-1} (1.5–300 THz). This setup provides measurements in high magnetic fields up to 16 T and low temperatures down to 2 K. The setup consists of a commercial FTIR spectrometer and a 16-T cryogen-free superconducting magnet coupled to the transmission probes designed for magneto-optical measurements with multiple detectors. Using various detectors, the setup spans the entire IR and partially the THz range. This aspect is particularly important because it enables the measurement of different types of samples from SMMs in the FIR region to germanium (Ge) in the NIR region, as demonstrated in the magneto-optical measurements section. Another novelty of the setup lies in the usage of a cryogen-free superconducting magnet.

II. Experimental Setup

Our FTIR magneto-spectroscopic setup, shown in Fig. 1, is based on a commercially available FTIR spectrometer Bruker Vertex 80v (Bruker Corporation, Billerica, USA) and a 16-T cryogen-free superconducting magnet (Cryogenic Ltd., London, U.K.). We have engineered custom optics to couple the spectrometer with the superconducting magnet, incorporating optical coupling and transmission probes (A, B) for multiple detectors. Additionally, the setup includes a home-built movable table housing the FTIR spectrometer, optical coupling, and detectors. The table, composed of aluminum profiles (Bosch Rexroth AG, Lohr am Main, Germany), ensures easy transfer and precise alignment of the setup due to its compatibility with the magnet frame, which is outfitted with an automatic motion mechanism originally designed for THz-FRaScan-EPR configuration [44], [45].

A. Beam Propagation

Fig. 2 presents the schematic of the FTIR magneto-spectroscopic setup, detailing beam propagation through two detector placement configurations. The beam originates from the spectrometer's source, passing through the aperture (APT = 8 mm) and beamsplitter (BMS) of the Michelson interferometer. The parallel beam is then guided through a spectrometer's output (OUT 2) toward the optical coupling, where it is reflected at a 90° angle by a parabolic mirror,

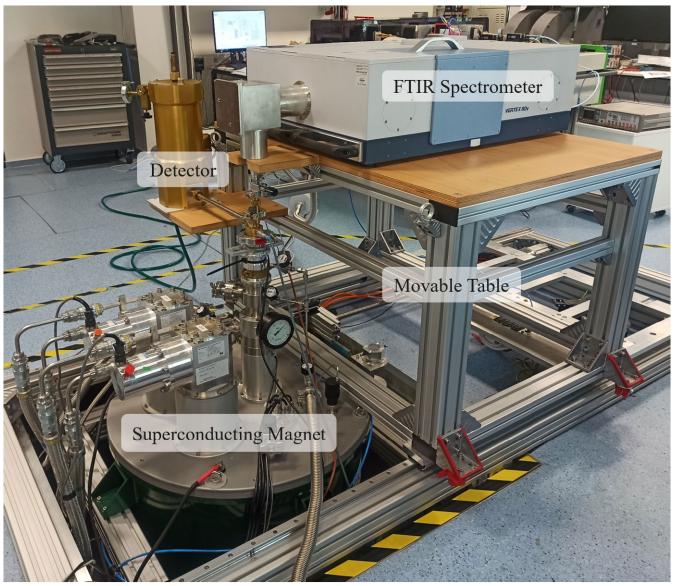

Fig. 1. Photograph of the FTIR magneto-spectroscopic setup at the Central European Institute of Technology, Brno University of Technology (CEITEC BUT). The setup shown in the photograph is in the configuration with Probe A and 1.6-K standard bolometer system.

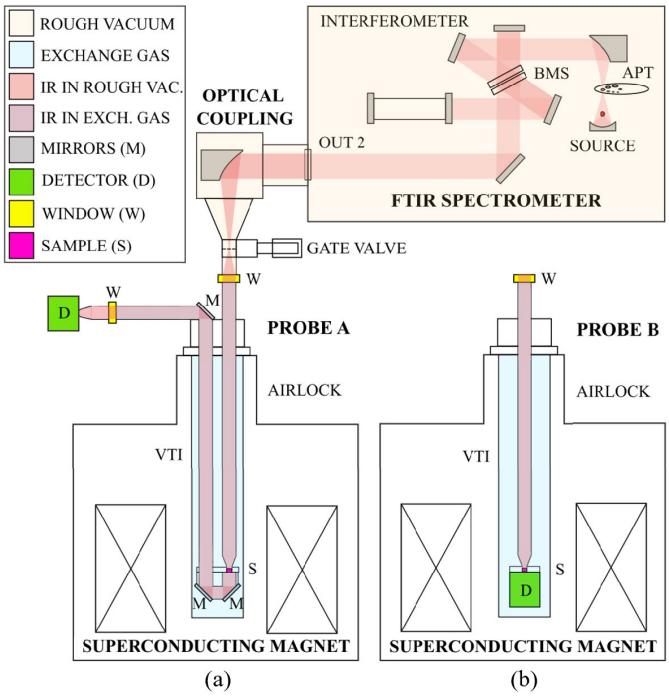

Fig. 2. The schematic of the FTIR magneto-spectroscopic setup shows the beam propagation through the setup in two configurations of the detector location. (a) Probe A, inserted into the superconducting magnet, is designed for the detector located outside the magnet and (b) Probe B is designed for the detector located inside the magnet. (VTI in the figure stands for VTI, BMS stands for beamsplitter, and APT stands for aperture.)

and focused to a gate valve. Upon closing the gate valve, the spectrometer, and optical coupling are evacuated to approximately 2 mbar pressure to reduce radiation losses caused by absorption in water vapor. This rough vacuum reaches the probe's window when the transmission probe is connected and the gate valve is reopened. After inserting the transmission probe through an airlock into the superconducting magnet's variable temperature insert (VTI), the probe is filled by helium gas. The setup's windows, made of 35 μm thick mylar foil, keep the helium gas inside the probe, separating it from the optical coupling and surrounding environment. Two transmission probes can be attached to the optical coupling.

1) Probe A: In this configuration, the detector (D) is placed outside the magnet, see Fig. 2(a). The beam enters the first tube and passes through the window (W). Then, it is transmitted through a sample (S) centrally located within the magnetic field. At the bottom of the probe, the transmitted beam is reflected by two 90° flat mirrors (M) and propagates up through a second tube. At the end of the second tube, another 90° flat mirror (M) is located, which reflects it to a third, horizontal, tube. At the end of this tube, the beam passes through another window (W) and goes to the detector (D).

2) Probe B: In this configuration, the detector (D) is placed inside the superconducting magnet, see Fig. 2(b). The beam enters the tube through the window (W), propagating toward a sample (S) located in the magnetic field's center. The transmitted beam from the sample (S) goes to the detector (D) positioned below the sample.

More details on Probes A and B will be described in Section III.

III. Setup Design and Components

In designing the setup's custom components, priority was given to using non-magnetic materials like brass, bronze, aluminum, and non-magnetic stainless steel (316 L). This choice mitigates complications from the magnet's stray fields. Another selection criterion for materials was suitability for cryogenic temperatures. The setup's components are sealed with o-rings ensuring rough vacuum conditions.

A. FTIR Spectrometer

The Bruker Vertex 80v spectrometer is designed for spectroscopic measurements under vacuum conditions, being supplied with an oil-free scroll vacuum pump. Standard configuration provides apodized spectral resolution of better than 0.2 cm^{-1}. The spectrometer is currently equipped with.

1) Sources: Standard MIR source (Globar), and NIR source (tungsten halogen lamp).

2) Beamsplitters (BMS): CaF_2 for NIR range, standard KBr for MIR range, Mylar Multilayer for FIR range.

3) Detectors: There are standard detectors operating at room temperature supplied together with the spectrometer: NIR InGaAs, MIR-DTGS (deuterated triglycine sulfate), and FIR-DTGS. Besides additional commercially available detectors operating at low temperatures can be connected to the spectrometer: a pumped LHe-cooled 1.6 K standard bolometer system (Infrared Laboratories, Tuscon, USA) for the FIR range, and a sealed 4.2 K general purpose bolometer with 3 mm diamond absorber (Infrared Laboratories, Tuscon, USA) for the FIR, MIR, and NIR ranges, which is designed to operate inside the superconducting magnet.

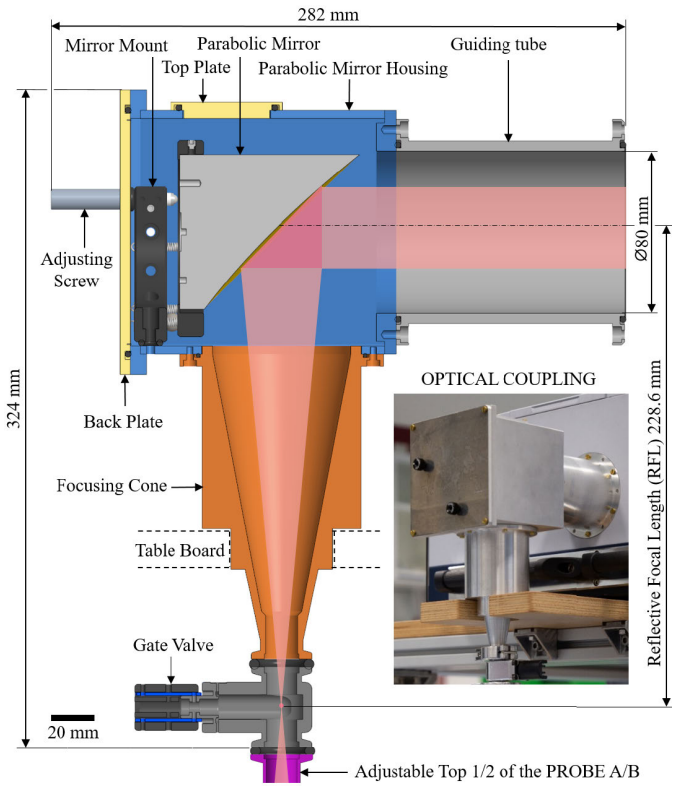

Fig. 3. Scheme of the optical coupling design. The optical coupling reflects the parallel beam from the spectrometer using a parabolic mirror and focuses it to Probe A or B inserted into the superconducting magnet.

B. Superconducting Magnet

A cryogen-free superconducting magnet is a primary choice for research facilities without cryogenics infrastructure. Our setup utilizes 16 T cryogen-free superconducting solenoid magnet equipped with two pulse cryocoolers and integrated VTI with a ⌀50 mm sample space, which enables control of the temperature T inside the magnet between $T = 1.8$–320 K. The VTI incorporates a home-built airlock port for probe insertion, avoiding contamination of the closed-cycle helium environment by pumping and flushing the probe space before sliding into the operation position via the opened VTI valve [44].

C. Optical Coupling

The optical coupling (see Fig. 3) is designed to reflect the parallel beam from the spectrometer using a parabolic mirror and focus it on the transmission probe inserted into the superconducting magnet. Its main purpose is to enable alignment, ensuring effective coupling of the probes. It comprises a guiding tube connected to the spectrometer's output (OUT 2, as displayed in Fig. 2), a housing for the parabolic mirror, a focusing cone mounted on the bottom of the housing, and a gate valve VATLOCK (VAT group AG, Haag, Switzerland)

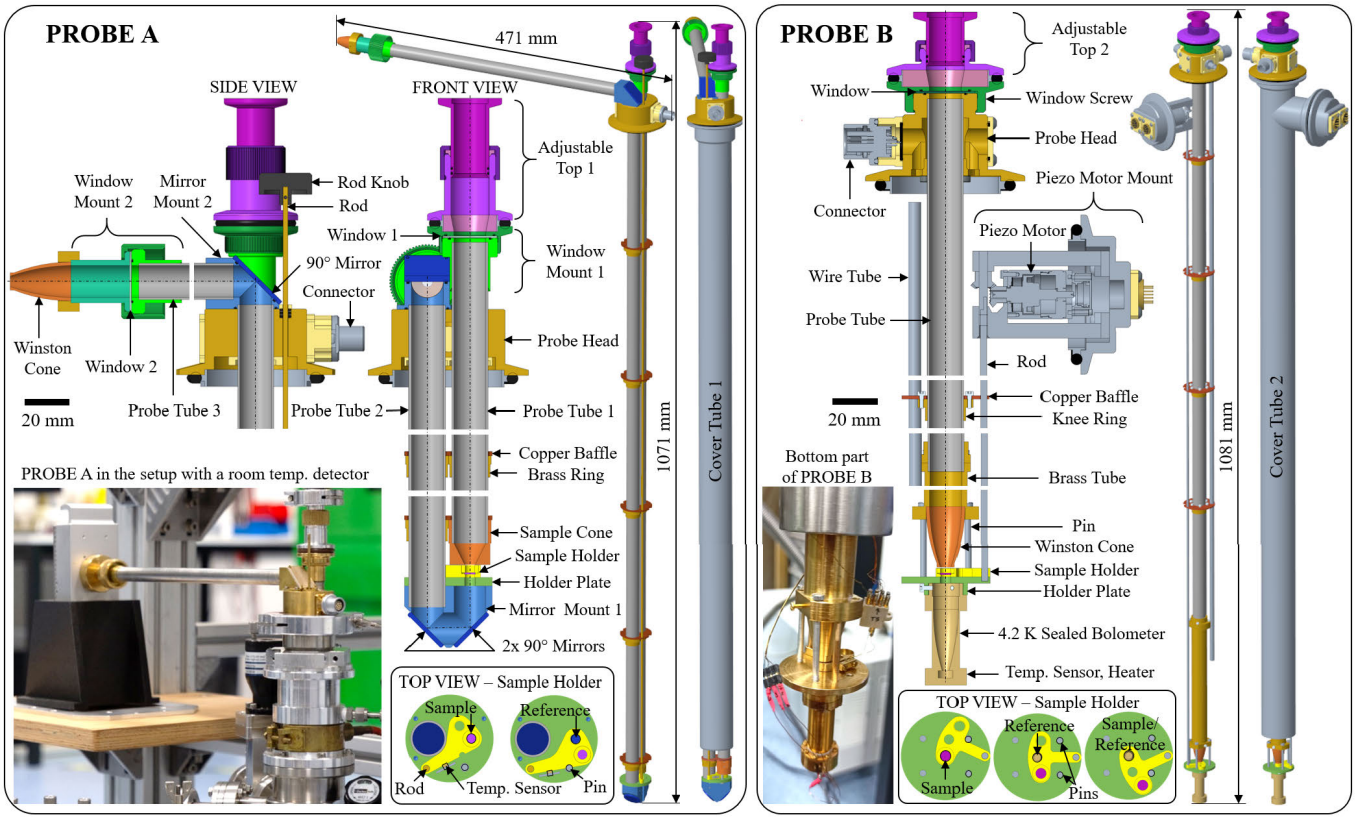

Fig. 4. Scheme of Probe A and B designs with multiple different views and photograph insets. These transmission probes are used as waveguides guiding the beam through a sample/reference in the magnetic field to the detector, which is in case of Probe A-external detection probe, placed outside the magnet, and in case of Probe B-internal detection probe, placed inside the superconducting magnet.

of inner diameter 15.1 mm with a manual actuator. Inside the mirror housing, a precision kinematic mirror mount (Thorlabs, Newton, NJ, USA) holds the ⌀76.2 mm 90° off-axis gold-coated parabolic mirror with Reflective Focal Length RFL = 228.6 mm (Thorlabs, Newton, NJ, USA). The parabolic mirror is aligned by two adjusting screws and through the opening covered by a top plate. A back plate serves to mount/dismount the parabolic mirror and the mirror mount. The parabolic mirror reflects the beam by 90° and focuses it at its focus point designed to be in the middle of the gate valve. The gate valve, mounted on the end of the focusing cone, separates the optical coupling from the probe A/B connected to the coupling by an adjustable top 1 or 2. When it is opened, the space until the window at the top of the probe is pumped to a rough vacuum (2 mbar) by the spectrometer's scroll pump.

D. Transmission Probes

Transmission probes, in other words, waveguides or light pipes, are tubes guiding the beam through a sample (reference) placed in the magnetic field to the detector. To reach stable cryogenic temperatures at a sample, it is necessary to reduce the heat flow from the top of the probe, which is at room temperature, to the probe tubes and a sample located inside the cryogenic helium environment. Therefore, the tubes (inner diameter of 15 mm) in our setup are made of non-magnetic stainless steel (316 L) due to its relatively low thermal conductivity compared with other materials traditionally used for waveguides, e.g., Nickel silver. These tubes were additionally polished inside to improve the reflectivity (to further improve reflectivity, it is possible in the future to coat the inside of the tubes with a thin layer of gold).

1) Probe A-External Detection Probe: Probe A (see Fig. 4) is connected to the gate valve flange by an adjustable top 1 which consists of two tubes sliding in each other to adjust the suitable height (center of the magnetic field at a sample). A window mount 1 is located below, where a window (mylar foil) is sealed by two o-rings. The thickness of the window can be up to 5 mm. Probe A consists of three non-magnetic stainless steel tubes/waveguides (probe tubes 1, 2, 3) attached to a probe head, which is hermetically connected to a non-magnetic stainless steel cover tube 1. The cover tube 1 secures the smooth loading of the probe into the airlock and the VTI. The probe head has two openings on the sides designed for connectors. There is one 11-pin connector DBEE104A056-130 (Fischer Connectors, Saint-Prex, Switzerland) used for connecting the temperature sensor Cernox CX-1050-SD-HT (LakeShore Cryotronics Inc., Westerville, USA) by Quad-Lead cryogenic wire 36 AWG (LakeShore Cryotronics Inc., USA). Probe tubes 1 and 2 are centered by five copper baffles that provide a lower heat transfer along the probe. The copper baffles are mounted to the brass rings attached to the probe tubes by hard soldering. On the end of the probe tube 1, a polished brass sample cone focusing the beam onto a sample is attached. The sample is placed in one of two slots of a sample holder. Another opening

is left empty to provide a measurement of a reference. The sample is in the Faraday configuration (i.e., in transmission mode, with the magnetic field parallel to the wave vector of the irradiation beam) and its vertical position is designed to be in the center of the magnetic field. Horizontally, the sample is 10 mm shifted from the center of the magnetic field due to the two-tube design. A sample can be a pressed powder pellet with ⌀5 mm or a wafer sample up to 8 mm in diameter that is fixed in the sample holder. The temperature sensor is mounted on the side of the sample holder, close to the sample. The shape of the sample holder is designed to provide precise switching between a sample and a reference by its sliding on a holder plate. On one side, a removable pin mounted to the holder plate is slotted to the sample holder to secure one extreme position, and the second extreme position is secured by probe tube 2, shown in Probe A inset in Fig. 4. Rotation of the sample holder is enabled by a brass rod mounted to the sample holder. A rod knob above the probe head is used to rotate the rod manually. After the beam passes through the sample/reference, it is guided by a mirror mount 1 with two 90° flat mirrors covered with a polished silver layer. They reflect the transmitted beam and guide it up to probe tube 2. Then, the beam is led by the probe tube 2 to another 90° flat mirror mounted onto a mirror mount 2. The beam guided by the mirror mount 2 propagates to a horizontal probe tube 3 toward the detector. On the end of the probe tube 3, window mount 2 seals a window 2 (mylar foil or other up to 5 mm) with an o-ring. When the room temperature detectors (InGaAs, MIR-DTGS, FIR-DTGS) are used, a Winston cone (Infrared Laboratories, Tuscon, USA) that concentrates the beam to a small spot, is attached to the end of the window mount 2. In the case of the LHe-cooled standard 1.6 K bolometer system, there is no need to use this cone since one is already incorporated into the bolometer's dewar.

The main advantage of the Probe A configuration, when the detector is placed externally (outside of the magnet), is that the temperature at a sample in the VTI can be varied (useful e.g., for materials with a phase transition). Moreover, the detectors are in this configuration further from the magnet, so measurements of the reference are unnecessary since the high magnetic fields do not influence the sensitivity of detectors. On the other side, when using LHe cooled 1.6 K standard bolometer system, regular filling of the bolometer's dewar with LHe is necessary for its operation. Also, since the end of the window mount 2/winston cone is not hermetically connected to the detector, the beam is going through the air approximately 5 cm, which causes absorption in water vapor in FIR spectra. The absorption in water vapor can be reduced by flowing nitrogen gas into this area. Another disadvantage is that the signal at the detector is lower due to losses caused by the relatively long optical path (approximately 2.5 m) of the beam propagating through the probe tubes. Also, the sample is not entirely in the horizontal center of the magnetic field, as the probe consists of two probe tubes.

2) Probe B-Internal Detection Probe: Probe B (see Fig. 4) is connected to the gate valve of the optical coupling by an adjustable top 2. Below, a window screw seals a mylar foil window with two o-rings. Probe B consists of one non-magnetic stainless steel tube/waveguide, a probe tube, attached to a probe head, which is connected to the cover tube 2 with a side port designed for inserting a piezo motor mount with a piezo step-motor LEGS Rotary LR23-50 (PiezoMotor Uppsala AB, Uppsala, Sweden). The piezo step-motor serves for automatic switching between a sample and a reference by rotation of a bronze rod mounted to a sample holder. The probe head has four openings on the sides designed for connectors. There is one 11-pin connector (DBEE104A056-130) for connecting the temperature sensor Cernox CX-1050-SD-HT (by Quad-Lead cryogenic wire 36 AWG), and heater (four 25 Ω resistors in series connected by a copper wire), and one four-pin connector SFE 102 A053-130 (Fischer Connectors, Saint-Prex, Switzerland) for connecting the sealed 4.2 K General Purpose Bolometer (Infrared Laboratories, Tuscon, USA) by Quad-Lead cryogenic wire 36 AWG. All wires are placed inside two wire tubes mounted along the probe tube. The temperature sensor and the heater are both mounted on the body of the sealed bolometer. The probe tube is centered by four copper baffles mounted to brass rings hard-soldered to the tube. On the bottom of the probe tube, a brass tube is mounted. Four pins with thread endings are inserted into the bottom of the brass tube and anchored in a holder plate. A Winston cone (Infrared Laboratories, Tuscon, USA) is mounted on the bottom of the brass tube. A sample holder with three slots for the samples/reference is placed under the Winston cone. The sample is again in the Faraday configuration, and its horizontal and vertical positions are designed to be in the center of the magnetic field.

It can be ⌀5 mm pressed powder pellet or wafer sample up to 8 mm in diameter, which is fixed in the sample holder. The shape of the sample holder is designed to provide precise switching between a sample and a reference. On both sides, two pins are slotted to the sample holder to secure extreme positions. The sample holder slides on the holder plate to which the sealed bolometer is mounted. After the beam passes through the sample/reference, it is guided by a Winston cone already incorporated in the sealed bolometer to its sensitive element. At the bottom of the sealed bolometer there are three pins for bias, signal, and ground. The wires from these pins go to the four-pin connector on the probe head. The ground wire is connected to the connector's frame, the bias wire goes to a bias box with two 9 V batteries, and the signal wire is connected to the input of a 200 MHz High Input Impedance Voltage Amplifier HVA-200M-40-F (FEMTO Messtechnik GmbH, Berlin, Germany). The output of the amplifier is connected to an A/D converter (Bruker Corporation, Billerica, USA) connected to the spectrometer.

A significant advantage of the Probe B configuration, when the detector is placed inside the magnet, is that we can use the LHe from the closed-cycle system used in the VTI for the operation of the sealed bolometer. Moreover, the signal at the detector is stronger due to lower losses of the beam since the optical path (approximately 1 m) is shorter than in Probe A. Additionally, by attaching the chip sample holder [44] instead of the sealed bolometer, Probe B can be used for testing graphene bolometer devices [46]. However,

the vibrations from the closed-cycle system might negatively influence the quality of the spectra. Another disadvantage is that since the operational temperature of the bolometer is 4.2 K, it is impossible to change the temperature on the sample and make temperature-dependent measurements. Also, the sealed bolometer is nearly in the center of the magnetic field (approximately 5 cm under the center of the magnetic field), so the reference measurements are needed due to the influence of the high magnetic field on the bolometer's sensitivity.

IV. Performance of the Setup

We have characterized the performance of the FTIR magneto-spectroscopic setup in several different configurations depending on the probe, source, beamsplitter, and detector choice. The results from these tests are summarized in Table I, in which typical operating spectral ranges for beamsplitters, detectors, operating temperature ranges for detectors, and possible sample temperatures are listed. We demonstrate the performance of the setup by the power spectrum, which depicts intensity versus wavenumber and the so-called 100% line, which is a typical indicator of the noise level of the spectroscopic system [3]. 100% line is obtained by measuring a transmission spectrum (spectrum 1) and then dividing it by a subsequent spectrum (spectrum 2). In the ideal case, the division should be a straight line at 100%. The deviation from this line represents the noise and instability of the system as a function of wavenumber (frequency) [8]. 100% line clearly displays the performance and workable setup range (fifth column of the table) for each configuration. To compare the performance between configurations in the specific IR range, 100% line spectra are plotted with the same y-axis range, $\pm 1\%$ for the NIR configurations, $\pm 10\%$ for the MIR and FIR configurations. These measurements were performed on an empty opening (reference) at zero magnetic field. All spectra were acquired with the same scanning time (10 min) and resolution (1 cm^{-1}). The interferometer scan speed f_{SCN} displayed in the power spectra was optimized for each detector based on its characteristics. As expected, the performance of the setup in configurations with room temperature FIR-DTGS and MIR-DTGS detectors is clearly worse than with using LHe-cooled detectors in the FIR and MIR ranges. In all presented configurations, mylar foil (35 μm) windows were used in the setup, but they can be easily replaced with windows made of other materials. We have chosen mylar due to its wide frequency range where it can be used. However, mylar caused typical absorptions around 1500 and 3000 cm^{-1} visible in the MIR range power spectra and noise peaks in 100% line (see Table S1 in the supplementary information).

V. Magneto-Optical Measurements

The functionality of the FTIR magneto-spectroscopic setup was demonstrated on two samples. The first sample was a representative of SMMs with very large ZFS, which was measured in the FIR range on the IR magneto-optical setup at GHMFL; results of these measurements can be found in [12], in the section called far infrared magnetic spectroscopy (FIRMS) for complex labeled as **3**. We chose this sample (identical 12 mg pellet) so we can compare the results obtained from our setup in the FIR region with those previously published. By the magneto-optical measurements of complex **3**, we tested the setup in the FIR region.

The second sample was a well-known indirect band gap semiconductor—Ge, measured in the NIR region to observe the magneto-optical response of its absorption edge. We chose Ge due to its well-studied band structure and the amount of available literature [55], [56].

A. Cobalt(II)-Based SIM

SMMs are molecules displaying slow relaxation of their magnetization of purely molecular origin [47]. Since their discovery in 1993 [48], their potential applications in the storage and processing of digital information have drawn the attention of the scientific community [49], [50]. An important class of SMMs is complexes containing only a single metal ion, often referred to as single-ion magnets (SIMs) [47]. SMMs, including SIMs, are usually characterized by a magnetic anisotropy constant D, also called the axial zero-field splitting (ZFS) [52], that represents the main anisotropic contribution to the spin Hamiltonian (SH). ZFS causes degeneration of spin states even at zero magnetic field. The SH also includes the rhombic ZFS contribution E and anisotropic Zeeman term defined by the g tensor. The knowledge of the SH parameters is vital to define the properties of the SMMs [15]. However, direct experimental determination of these parameters for SMMs with large ZFS, which are of current interest [10], [53], might be challenging. Besides, conventional MW ESR systems do not provide experimental access to the ESR transitions of SMMs with large ZFS. FTIR magneto-spectroscopy enables us to observe ESR transitions of SMMs with large ZFS, mainly based on transition metal complexes [10], [11], [12], [13], [14], [15], [16], or lanthanides [17], [18], and to determine ZFS directly from the spectra [35], [54]. For cobalt(II) complexes with $S = 3/2$, the ZFS between two Kramers doublets is equal to $2(D^2 + 3E^2)^{1/2}$. This energy gap is then directly observable in FTIR magneto-optical spectra as 2-D (when omitting rhombicity E).

The spectra of pressed powder pellet of pentacoordinate cobalt(II)-based complex **3** ($[\text{Co(L2)Cl}_2]$, where L2 = 2, 6-bis(1-dodecyl-1H-benzimidazole-2-yl)-pyridine (see Fig. S1 in the supplementary information), were recorded in Probe A configuration with 1.6 K standard bolometer system in the FIR region at $T = 2$ K and magnetic fields B up to 16 T. The spectra were measured with resolution 4 cm^{-1}, same as in [12] (see Fig. S2 and S3), and resolution 1 cm^{-1}, see Fig. 5 (see Fig. S4 and S5). Since the peaks are very narrow, resolution 1 cm^{-1} was found to be more suitable than resolution 4 cm^{-1}. The transmission spectra of the sample at magnetic field (T_B) were normalized by the zero-field transmission spectra of the sample (T_0), T_B/T_0. Normalized relative transmission spectra (see Fig. S2 and S4) are depicted in the form of a color map in Fig. 5 (see Fig. S3 and S5) for better identification of the ESR transitions. Color maps of the normalized relative transmission spectra show a clear field-dependence of one of the peaks starting at $\sim$186 cm^{-1} at zero magnetic field

TABLE I

ALL POSSIBLE CONFIGURATIONS OF THE FTIR MAGNETO-SPECTROSCOPIC SETUP ACCORDING TO THE CHOICE OF THE PROBE, SOURCE, BEAMSPLITTER, AND DETECTOR, WITH SPECTRAL AND SAMPLE TEMPERATURE RANGES, AND CORRESPONDING POWER SPECTRUM (INTENSITY VERSUS WAVENUMBER) TOGETHER WITH 100% LINE, OBTAINED AS THE DIVISION OF SPECTRUM 1 BY A SUBSEQUENT SPECTRUM 2. (*THIS RANGE OF THE BOLOMETER WAS PROVIDED BY THE MANUFACTURER, BUT THE BOLOMETER WORKED FAR ABOVE THIS RANGE)

Probe	Source	Beamsplitter range (cm^{-1})	Detector range (cm^{-1}) (Oper. temp.)	Setup range (cm^{-1})	Sample temp. (K)	Power spectrum	100% line
A	Tungsten	CaF_2 1,200 – 15,000	InGaAs 4,000 – 12,800 (Room Temp.)	**NIR** 4,000 – 10,000	2 – 320	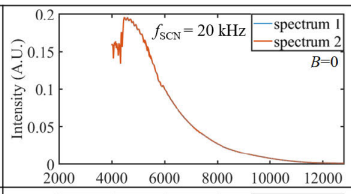	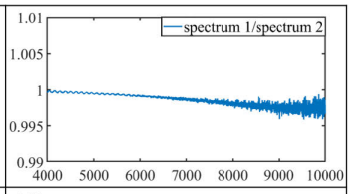
B	Tungsten	CaF_2 1,200 – 15,000	4.2 K Sealed Bolometer 10 – 2,000* (LHe-cooled)	**NIR** 2,000 – 8,000	4.2	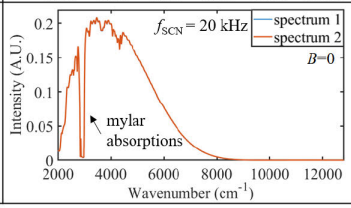	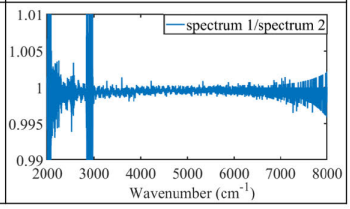
A	Globar	KBr 350 – 8,000	MIR-DTGS 250 – 12,000 (Room Temp.)	**MIR** 400 – 5,000	2 – 320	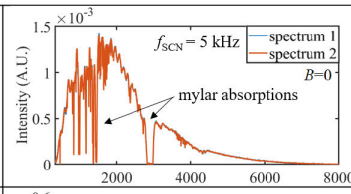	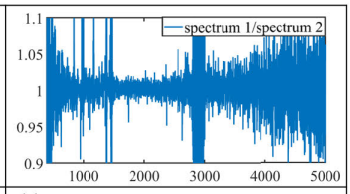
B	Globar	KBr 350 – 8,000	4.2 K Sealed Bolometer 10 – 2,000* (LHe-cooled)	**MIR** 400 – 4,000	4.2	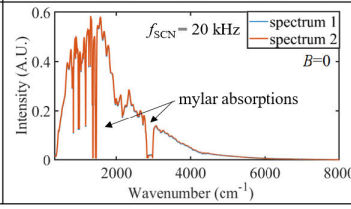	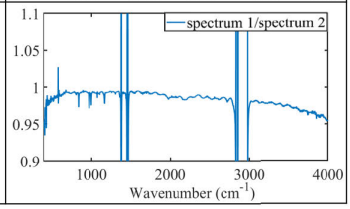
A	Globar	Mylar Multilayer 30 – 680	FIR-DTGS 10 – 700 (Room Temp.)	**FIR** 150 – 680	2 – 320	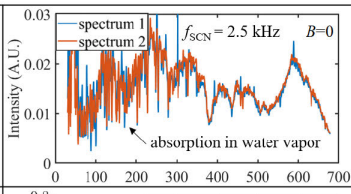	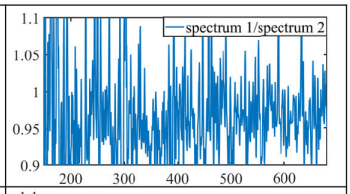
A	Globar	Mylar Multilayer 30 – 680	1.6 K Standard Bolometer 5 – 670 (LHe-cooled)	**FIR** 50 – 670	2 – 320	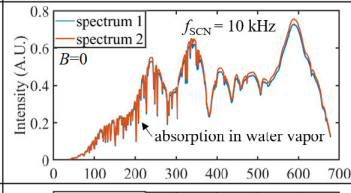	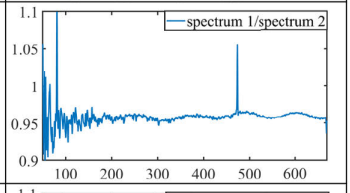
B	Globar	Mylar Multilayer 30 – 680	4.2 K Sealed Bolometer 10 – 2,000* (LHe-cooled)	**FIR** 50 – 680	4.2	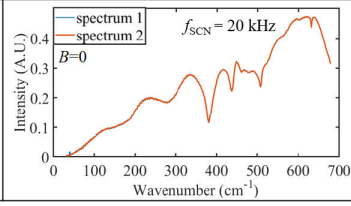	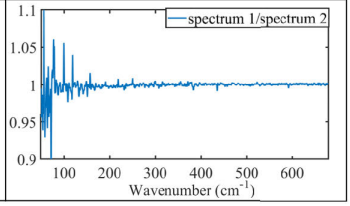

attributed to the ESR transition from $m_s = \pm 3/2$ to $m_s = \pm 1/2$ states. In Fig. 5, we applied the same simulation as in [12] calculated using the EasySpin Toolbox for Matlab [57] based on the SH and the parameters $E/D = 0.162$, $D = -89$ cm^{-1}, $g_{iso} = 2.1$. In addition, we normalized the data as T_B/T_{B+1} and applied the same simulation to confirm the peak position (see Fig. S5). Red color of the simulation represents the strongly allowed transitions; gray color indicates forbidden/weakly allowed transitions. The spectra obtained on our setup at CEITEC BUT shown in Fig. 5 are almost

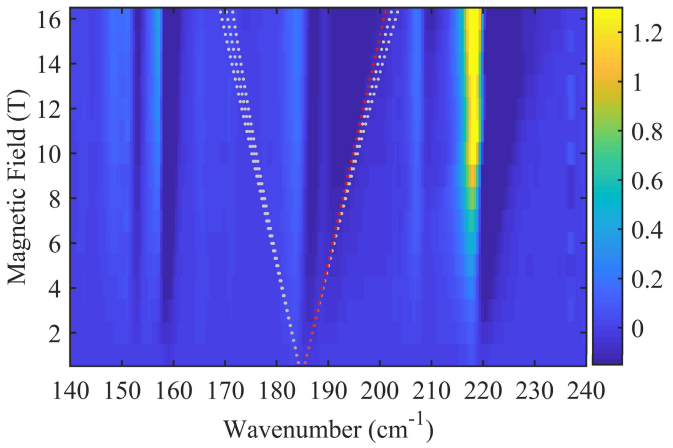

Fig. 5. Color map of normalized relative transmission spectra recorded on pressed powder pellet of **3** measured at $T = 2$ K, magnetic field up to 16 T, and resolution 1 cm^{-1} obtained on our FTIR magneto-spectroscopic setup. Simulations with the SH ($S = 3/2$, $D = -89$ cm^{-1}, $E/D = 0.162$, $g_{iso} = 2.1$) are shown as dotted lines. Red color represents the strongly allowed transitions; gray color indicates forbidden/weakly allowed transitions.

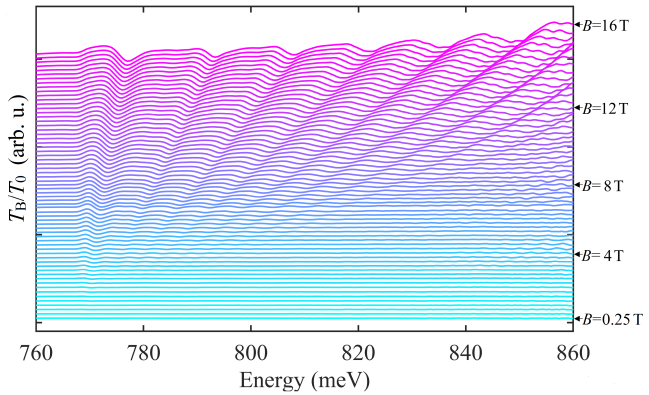

Fig. 6. Normalized relative transmission spectra, T_B/T_0, plotted with an offset for 64 values of applied magnetic fields from 0.25 to 16 T with step 0.25 T. The maxima correspond to individual inter-LL transitions, and the minima emerge due to the suppression of the zero-field absorption.

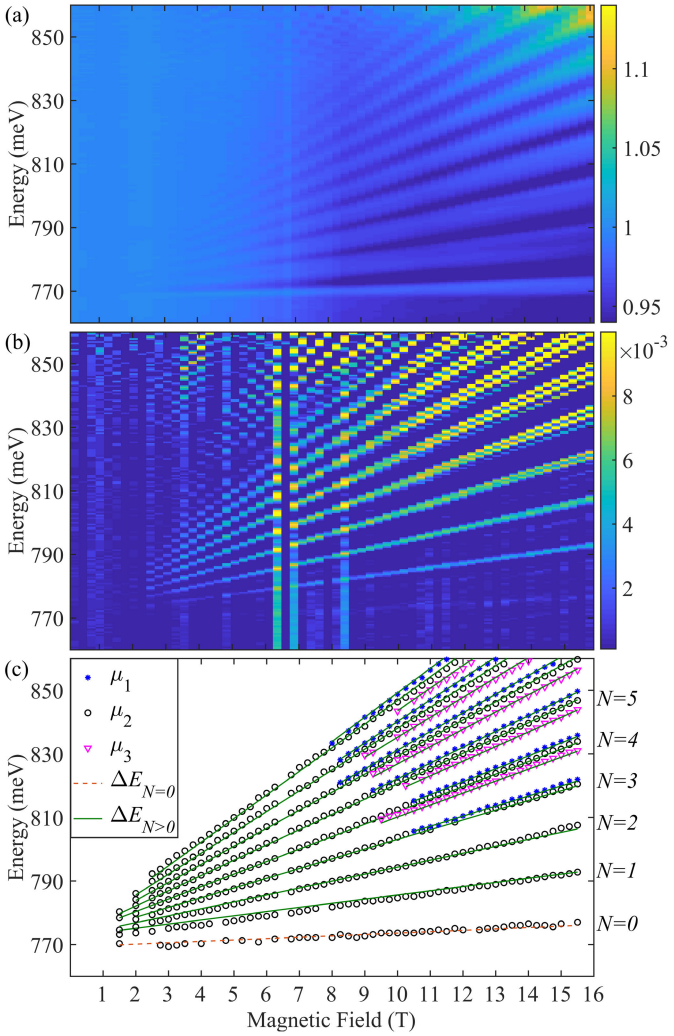

Fig. 7. (a) Color map of normalized relative transmission spectra from Fig. 6. (b) Color map of the second derivative of normalized relative transmission spectra from (a). (c) Minima of (b) fit with a model of LL transitions as described in the text. Three markers correspond to three values of reduced effective mass. The solid and dashed lines correspond to two values of ΔE_N.

identical to those obtained at GHMFL [see Fig. S3(b)]. In all color maps, the tendency toward the yellow color means the absorption is suppressed by the magnetic field, whereas the dark blue color means the absorption is induced by the magnetic field.

B. Germanium

Using the FTIR magneto-spectroscopy, we can probe the band structure, e.g., LLs, and elucidate the electronic properties of 2-D materials such as graphene [19], [20], [21], [22], [23], or semiconductors such as Ge [55], [56].

The magneto-optical spectra were acquired on a very weakly p-type galium-doped Ge ($\rho = 11$ Ωcm, $p = 2 \times 10^{14}$ cm^3) (100) wafer at 5 K in the magnetic field B up to 16 T with Probe A and InGaAs room temperature detector in the NIR region. Fig. 6 shows normalized relative transmission spectra (T_B/T_0) of Ge measured with resolution 8 cm^{-1} at 64 values of applied magnetic fields B from 0.25 to 16 T with step 0.25 T plotted with an offset for clarity. The spectra are shown in the range of absorption edge of Ge at low temperatures. The maxima correspond to individual inter-LL transitions. The minima correspond to the suppression of zero-field absorption. Normalized relative transmission spectra from Fig. 6 were visualized as a color map shown in Fig. 7(a). Fig. 7(b) displays a color map of the second derivative of these normalized relative transmission spectra to enhance fine structures, e.g., the splitting of LL transitions. The maxima of the signal in Fig. 7(b) are shown in Fig. 7(c). They were analyzed using the model of transitions between LLs of parabolic bands [58]

$$E_N = \Delta E_N + \left(N + \frac{1}{2}\right)\hbar\omega_c$$

where $N = 0, 1, 2, \ldots$ is the index of a LL, ΔE_N is the energy value at $B = 0$, $\omega_c = eB/\mu$ is the cyclotron frequency, e is the elementary charge, and μ is the reduced effective mass. Parabolicity of the bands leads to the linear dependence of the energy of absorption lines to the magnetic field, which is well fulfilled in the whole measured range. The model employs three different reduced effective masses,

$\mu_1 = (0.128 \pm 0.015)$ m, $\mu_2 = (0.132 \pm 0.016)$ m, $\mu_3 = (0.138 \pm 0.014)$ m where m is the free electron mass, to account for the small splitting of LL, which becomes apparent for $N > 3$. The LL with $N = 0$ has a different value of $\Delta E_{N=0} = 769$ meV than for $N > 3$, $\Delta E_{N>0} = 773$ meV. The latter indicates that a different phonon mediates $N = 0$ transition than $N > 0$ transitions. Considering the value of the band gap of Ge at low temperatures of 741 meV [59], the energy of phonons amounts to 28 meV for $N = 0$ transition and 32 meV for $N > 0$ transitions. The three values of reduced effective masses compare well with the electron effective masses obtained by Dresselhaus et al. [55]for the sample with a magnetic field tilted by a few degrees from the (001) direction, see Fig. 5. Surprisingly, the obtained effective masses compare well with the electron effective mass rather than with the reduced effective mass $1/\mu = 1/m_{\text{hh}} + 1/m_e$, which is expected for an indirect transition between the heavy hole band with effective hole mass $m_{\text{hh}} = 0.29$ m and the conduction band with effective electron mass $m_e = 0.13$ m for B in 001 direction. We tentatively interpret this observation as a transition between localized hole states (with a very large effective mass) to the conduction band.

VI. Conclusion

In this article, we have described in detail the versatile FTIR magneto-spectroscopic setup operating in the range 50–10 000 cm^{-1}, temperatures between 2 and 320 K, and magnetic fields up to 16 T located at the Central European Institute of Technology of Brno University of Technology (CEITEC BUT). We have tested the performance of the FTIR magneto-spectroscopic setup at zero magnetic field for various configurations to determine a workable setup range summarized in Table I. The functionality of the setup has been demonstrated on magneto-optical measurements of cobalt(II)-based SIM in the FIR region and Ge in the NIR region. The measurements of SIM have shown that the setup provides high-quality spectra and results comparable to those performed on a similar setup at GHMFL. In Ge, we observed indirect inter-band transitions between LLs and analyzed them with a model yielding three values of reduced effective masses.

In the context of prospective advancements, the flexibility of the FTIR magneto-spectroscopic setup enables further development and improvements, such as the implementation of new sample holders for different types of measurements, internal coating of waveguides with a layer of gold to further enhance the transmission, etc. Our group focuses on the studies of SMMs and high-spin coordination compounds with large ZFS, including transition metals and lanthanides, exploring the physics behind their behavior still rarely reported at those energy ranges. Furthermore, the presented versatile setup allows performing field-induced measurements on 2-D devices [46], e.g., by shifting the Fermi level in semiconductors, and electrically detected magnetic resonance (EDMR) [60], which may lead to interesting discoveries. Moreover, we are interested in exploring the properties of topological insulators [24] and Weyl semimetals [27], which are known to exhibit exotic electronic properties under applied magnetic fields.

Thanks to its relatively simple design and implementation of a cryogen-free superconducting magnet, the presented FTIR magneto-spectroscopic setup paves the way for other research institutions without the LHe infrastructure to perform IR magneto-optical experiments in high magnetic fields. Data in this article will be available on request.

Acknowledgment

The authors would like to thank all members of the MOTeS CEITEC Group for useful discussions and comments during the development of the setup, namely Dr. Oleksii Laguta for help with the electronics and laboratory equipment and Associate Professor. Ivan Šalitroš and Ing. Jana Juráková for providing the SIM sample. Then, they would like to thank Dominik Varga (CEITEC Nano research infrastructure, Brno, Czech Republic) for the fabrication of the setup components in the mechanical workshop. They would especially like to thank RNDr. Milan Orlita, Ph.D. (Grenoble High Magnetic Field Laboratory (GHMFL), Grenoble, France) for helpful advice during the design and optimization of the setup and fruitful discussions over the results of magneto-optical measurements and Ing. Aleš Srnka, CSc. (Institute of Scientific Instruments of the Czech Academy of Sciences, Brno, Czech Republic) for help in the organization of measurements.

References

[1] A. A. Christy, Y. Ozaki, and V. G. Gregoriou, *Modern Fourier Transform Infrared Spectroscopy*. New York, NY, USA: Elsevier, 2001.

[2] M. R. Derrick, D. Stulik, and J. M. Landry, *Infrared Spectroscopy in Conservation Science*. Los Angeles, CA, USA: Getty Conservation Institute, 1999.

[3] P. R. Griffiths and J. A. De Haseth, *Fourier Transform Infrared Spectrometry*, 2nd ed. Hoboken, NJ, USA: Wiley, 2007.

[4] Y. Ozaki, "Infrared spectroscopy—Mid-infrared, near-infrared, and far-infrared/terahertz spectroscopy," *Anal. Sci.*, vol. 37, no. 9, pp. 1193–1212, Sep. 2021.

[5] Y.-S. Lee, *Principle of Terahertz Science and Technology*. New York, NY, USA: Springer, 2009.

[6] S. L. Dexheimer, *Terahertz Spectroscopy: Principles and Applications*. Boca Raton, FL, USA: CRC Press, 2008.

[7] H. H. Mantsch and D. Naumann, "Terahertz spectroscopy: The renaissance of far infrared spectroscopy," *J. Mol. Struct.*, vol. 964, nos. 1–3, pp. 1–4, Feb. 2010.

[8] W. J. Padilla, Z. Q. Li, K. S. Burch, Y. S. Lee, K. J. Mikolaitis, and D. N. Basov, "Broadband multi-interferometer spectroscopy in high magnetic fields: From THz to visible," *Rev. Sci. Instrum.*, vol. 75, no. 11, pp. 4710–4717, Nov. 2004.

[9] D. N. Basov, R. D. Averitt, D. van der Marel, M. Dressel, and K. Haule, "Electrodynamics of correlated electron materials," *Rev. Mod. Phys.*, vol. 83, no. 2, pp. 471–541, Jun. 2011.

[10] Y. Rechkemmer et al., "A four-coordinate cobalt(II) single-ion magnet with coercivity and a very high energy barrier," *Nature Commun.*, vol. 7, no. 1, p. 10467, Feb. 2016.

[11] H. Bamberger et al., "Iron(II), cobalt(II), and nickel(II) complexes of bis (sulfonamido) benzenes: Redox properties, large zero-field splittings, and single-ion magnets," *Inorganic Chem.*, vol. 60, no. 5, pp. 2953–2963, Mar. 2021.

[12] J. Juráková et al., "Pentacoordinate cobalt(II) single ion magnets with pendant alkyl chains: Shall we go for chloride or bromide?" *Inorganic Chem. Frontiers*, vol. 9, no. 6, pp. 1179–1194, 2022.

[13] N. Malinová et al., "Magnetization slow dynamics in mononuclear Co(II) field-induced single-molecule magnet," *Crystal Growth Des.*, vol. 23, no. 4, pp. 2430–2441, Apr. 2023.

[14] J.-J. Liu et al., "Determination of zero-field splitting in Co^{2+} halide complexes with magnetic and far-IR measurements," *Dalton Trans.*, vol. 46, no. 23, pp. 7408–7411, 2017.

[15] E. Y. Misochko et al., "Purely spectroscopic determination of the spin Hamiltonian parameters in high-spin six-coordinated cobalt(II) complexes with large zero-field splitting," *Inorganic Chem.*, vol. 58, no. 24, pp. 16434–16444, Dec. 2019.

[16] D. H. Moseley et al., "Spin–phonon couplings in transition metal complexes with slow magnetic relaxation," *Nature Commun.*, vol. 9, no. 1, p. 2572, Jul. 2018.

[17] R. Marx et al., "Spectroscopic determination of crystal field splittings in lanthanide double deckers," *Chem. Sci.*, vol. 5, no. 8, pp. 3287–3293, 2014.

[18] J. G. C. Kragskow et al., "Analysis of vibronic coupling in a 4f molecular magnet with FIRMS," *Nature Commun.*, vol. 13, no. 1, p. 825, Feb. 2022.

[19] P. Neugebauer, M. Orlita, C. Faugeras, A.-L. Barra, and M. Potemski, "How perfect can graphene be?" *Phys. Rev. Lett.*, vol. 103, no. 13, 2009, Art. no. 136403.

[20] Z. Jiang et al., "Infrared spectroscopy of Landau levels of graphene," *Phys. Rev. Lett.*, vol. 98, no. 19, May 2007, Art. no. 197403.

[21] I. O. Nedoliuk, S. Hu, A. K. Geim, and A. B. Kuzmenko, "Colossal infrared and terahertz magneto-optical activity in a two-dimensional dirac material," *Nature Nanotechnol.*, vol. 14, no. 8, pp. 756–761, Aug. 2019.

[22] M. Orlita et al., "Approaching the dirac point in high-mobility multilayer epitaxial graphene," *Phys. Rev. Lett.*, vol. 101, no. 26, Dec. 2008, Art. no. 267601.

[23] I. Crassee et al., "Giant Faraday rotation in single- and multilayer graphene," *Nature Phys.*, vol. 7, no. 1, pp. 48–51, Jan. 2011.

[24] I. Mohelský et al., "Landau level spectroscopy of Bi_2Se_3," *Phys. Rev. B, Condens. Matter*, vol. 102, no. 8, pp. 1–11, 2020.

[25] M. Orlita et al., "Magneto-optics of massive dirac fermions in bulk Bi_2Se_3," *Phys. Rev. Lett.*, vol. 114, no. 18, 2015, Art. no. 186401.

[26] K. K. Tikuišis et al., "Landau level spectroscopy of the PbSnSe topological crystalline insulator," *Phys. Rev. B, Condens. Matter*, vol. 103, no. 15, Apr. 2021, Art. no. 155304.

[27] S. Polatkan et al., "Magneto-optics of a Weyl semimetal beyond the conical band approximation: Case study of TaP," *Phys. Rev. Lett.*, vol. 124, no. 17, Apr. 2020, Art. no. 176402.

[28] F. Hütt et al., "Terahertz transmission through TaAs single crystals in simultaneously applied magnetic and electric fields: Possible optical signatures of the chiral anomaly in a Weyl semimetal," *Results Phys.*, vol. 15, Dec. 2019, Art. no. 102630.

[29] A. D. LaForge et al., "Sum rules and interlayer infrared response of the high temperature $YBa_2Cu_3O_y$ superconductor in an external magnetic field," *Phys. Rev. Lett.*, vol. 101, no. 9, Aug. 2008, Art. no. 097008.

[30] M. Šindler, F. Kadlec, and C. Kadlec, "Onset of a superconductor-insulator transition in an ultrathin NbN film under in-plane magnetic field studied by terahertz spectroscopy," *Phys. Rev. B, Condens. Matter*, vol. 105, no. 1, Jan. 2022, Art. no. 014506.

[31] A. I. Smirnov, T. I. Smirnova, R. L. MacArthur, J. A. Good, and R. Hall, "Cryogen-free superconducting magnet system for multifrequency electron paramagnetic resonance up to 12.1 T," *Rev. Sci. Instrum.*, vol. 77, no. 3, Mar. 2006, Art. no. 035108.

[32] R. Hirose, S. Hayashi, and K. Shibutani, "Cryogen-free superconducting magnet," *Kobelco Technol. Rev.*, no. 27, pp. 18–22, 2007.

[33] S. Awaji et al., "New 25 T cryogen-free superconducting magnet project at Tohoku University," *IEEE Trans. Appl. Supercond.*, vol. 24, no. 3, pp. 1–5, Jun. 2014.

[34] K. Holldack and A. Schnegg, "THz electron paramagnetic resonance/THz spectroscopy at BESSY II," *J. Large-Scale Res. Facilities*, vol. 2, pp. 1–5, 2016.

[35] J. Nehrkorn, K. Holldack, R. Bittl, and A. Schnegg, "Recent progress in synchrotron-based frequency-domain Fourier-transform THz-EPR," *J. Magn. Reson.*, vol. 280, pp. 10–19, Jul. 2017.

[36] R. P. S. M. Lobo, J. D. LaVeigne, D. H. Reitze, D. B. Tanner, and G. L. Carr, "Performance of new infrared beamline U12IR at the national synchrotron light source," *Rev. Sci. Instrum.*, vol. 70, no. 7, pp. 2899–2904, Jul. 1999.

[37] K. Takehana et al., "Far-infrared spectroscopy in high magnetic fields," *Phys. B, Condens. Matter*, vol. 216, nos. 3–4, pp. 354–357, Jan. 1996.

[38] K. M. Kojima et al., "New Josephson plasma modes in underdoped $YBa_2Cu_3O_{6.6}$ induced by a parallel magnetic field," *Phys. Rev. Lett.*, vol. 89, no. 24, 2002, Art. no. 247001.

[39] C. Kadlec et al., "Electromagnon in ferrimagnetic ϵ–Fe_2O_3 nanograin ceramics," *Phys. Rev. B, Condens. Matter*, vol. 88, no. 10, Sep. 2013, Art. no. 104301.

[40] J. L. M. van Mechelen et al., "Spin resonance in $EuTiO_3$ probed by time-domain gigahertz ellipsometry," *Phys. Rev. Lett.*, vol. 106, no. 21, 2011, Art. no. 217601.

[41] M. Schubert et al., "Terahertz electron paramagnetic resonance generalized spectroscopic ellipsometry: The magnetic response of the nitrogen defect in 4H-SiC," *Appl. Phys. Lett.*, vol. 120, no. 10, Mar. 2022, Art. no. 102101.

[42] P. Kühne, C. M. Herzinger, M. Schubert, J. A. Woollam, and T. Hofmann, "Invited article: An integrated mid-infrared, far-infrared, and terahertz optical Hall effect instrument," *Rev. Sci. Instrum.*, vol. 85, no. 7, Jul. 2014, Art. no. 071301.

[43] P. Kühne, N. Armakavicius, V. Stanishev, C. M. Herzinger, M. Schubert, and V. Darakchieva, "Advanced terahertz frequency-domain ellipsometry instrumentation for in situ and ex situ applications," *IEEE Trans. THz Sci. Technol.*, vol. 8, no. 3, pp. 257–270, May 2018.

[44] A. Sojka et al., "Sample holders for sub-THz electron spin resonance spectroscopy," *IEEE Trans. Instrum. Meas.*, vol. 71, pp. 1–12, 2022.

[45] O. Laguta, A. Sojka, A. Marko, and P. Neugebauer, "Rapid scan ESR: A versatile tool for the spin relaxation studies at (sub)THz frequencies," *Appl. Phys. Lett.*, vol. 120, no. 12, Mar. 2022, Art. no. 120502.

[46] L. S. Marie et al., "Nanostructured graphene for nanoscale electron paramagnetic resonance spectroscopy," *J. Phys., Mater.*, vol. 3, no. 1, Jan. 2020, Art. no. 014013.

[47] J. M. Frost, K. L. M. Harriman, and M. Murugesu, "The rise of 3-D single-ion magnets in molecular magnetism: Towards materials from molecules?" *Chem. Sci.*, vol. 7, no. 4, pp. 2470–2491, 2016.

[48] R. Sessoli, D. Gatteschi, A. Caneschi, and M. A. Novak, "Magnetic bistability in a metal-ion cluster," *Nature*, vol. 365, no. 6442, pp. 141–143, Sep. 1993.

[49] D. Gatteschi, A. Cornia, M. Mannini, and R. Sessoli, "Organizing and addressing magnetic molecules," *Inorganic Chem.*, vol. 48, no. 8, pp. 3408–3419, Apr. 2009.

[50] D. Gatteschi, R. Sessoli, and J. Villain, *Molecular Nanomagnets*. London, U.K.: Oxford Univ. Press, 2006.

[51] C. Benelli and D. Gatteschi, *Introduction to Molecular Magnetism: From Transition Metals to Lanthanides*. Hoboken, NJ, USA: Wiley, 2015.

[52] J. Telser, "Zero-field splittings," *EMagRes*, vol. 6, pp. 207–234, Jun. 2017.

[53] F.-S. Guo et al., "Magnetic hysteresis up to 80 kelvin in a dysprosium metallocene single-molecule magnet," *Science*, vol. 362, no. 6421, pp. 1400–1403, 2018.

[54] R. Winpenny and G. Aromí, *Single-Molecule Magnets and Related Phenomena*. New York, NY, USA: Springer, 2006.

[55] G. Dresselhaus, A. F. Kip, and C. Kittel, "Cyclotron resonance of electrons and holes in silicon and germanium crystals," *Phys. Rev.*, vol. 98, no. 2, pp. 368–384, Apr. 1955.

[56] Y. Yu and M. Cardona, *Fundamentals of Semiconductors, Graduate Texts in Physics*, 4th ed. Berlin, Germany: Springer-Verlag, 2010.

[57] S. Stoll and A. Schweiger, "EasySpin, a comprehensive software package for spectral simulation and analysis in EPR," *J. Magn. Reson.*, vol. 178, no. 1, pp. 42–55, Jan. 2006.

[58] F. R. Kessler and J. Metzdorf, "Landau level spectroscopy: Interband effects and Faraday rotation," in *Modern Problems in Condensed Matter Sciences*, vol. 27, no. 1. Amsterdam, The Netherlands: Elsevier, 1991, ch. 11, pp. 579–675.

[59] Y. P. Varshni, "Temperature dependence of the energy gap in semiconductors," *Physica*, vol. 34, no. 1, pp. 149–154, Jan. 1967.

[60] A. Solodovnyk et al., "Spin dynamics of exchange-coupled nitrogen donors in heavily doped n-type 15R SiC monocrystals: Multifrequency EPR and EDMR study," *Phys. Rev. B, Condens. Matter*, vol. 107, no. 15, Apr. 2023, Art. no. 155202.

Jana Dubnická Midlíková received the bachelor's and master's degrees in physical engineering and nanotechnology from the Brno University of Technology (BUT), Brno, Czech Republic, in 2016 and 2018, respectively. She is currently pursuing the Ph.D. degree with the Central European Institute of Technology (CEITEC), BUT, under the supervision of Petr Neugebauer with the Magneto-Optical and Terahertz Spectroscopy (MOTeS) Group.

Her research interests include the development of FTIR spectroscopy in high magnetic fields and the application of this method to study single-molecule magnets and 2-D materials.

Matúš Šedivý received the master's degree in microelectronics engineering from the Brno University of Technology (BUT), Brno, Czech Republic, in 2017. He is currently pursuing the Ph.D. degree with the MOTeS Group with the topic of Fast Electron Spin Resonance Spectroscopy Measurement System at Terahertz Frequencies.

He focuses on the development of software for automated control of a custom-built HF-ESR spectrometer and upgrade of hardware to expand capabilities of the spectrometer. His research interests include application of ESR to study semiconductors.

Antonín Sojka received the Ph.D. degree in advanced nanotechnologies and microtechnologies with the Central European Institute of Technology, Brno University of Technology (BUT), Brno, Czech Republic, in 2022.

During his Ph.D. studies, he successfully developed a novel terahertz magnetic resonance spectrometer for spin dynamics investigations. He is currently a Post-Doctoral internship with the University of California at Santa Barbara, Santa Barbara, CA, USA, under the supervision of prof. Mark Sherwin with a focus on developing new high-field ESR experiments powered by the free electron laser at UCSB.

Vinicius Tadeu Santana received the Ph.D. degree in applied physics from the University of Paulo, Paulo, Brazil, in 2016, working with exchange-coupled molecular compounds using ESR spectroscopy supervised by Prof. O. R. Nascimento.

He is currently a Junior Research Fellow with the Central European Institute of Technology, Brno University of Technology, Brno, Czech Republic, and a Team Member of Associate Professor with P. Neugebauer's Group, working with applications of ESR in molecular spin systems and solid-state magnetic materials.

Adam Dubroka received the Ph.D. degree in solid-state physics with Masaryk University, Brno, Czech Republic, in 2006.

He spent five years as a Post-Doctoral with the Group of Prof. C. Bernhard in Fribourg, Switzerland, focusing on the ellipsometry of strongly correlated materials, e.g., high-temperature superconductors. Since 2012, he has been an Associate Professor with Masaryk University.

Currently, he focuses on the electronic properties of magnetic materials studied by ellipsometry and dimensional crossover in magnetic heterostructures grown by pulsed laser deposition.

Petr Neugebauer received the Ph.D. degree with Marie Curie fellowship from the Physics of Condensed Matter and Radiation, Grenoble High Magnetic Field Laboratory, Grenoble, France, in 2010.

After his two years Post-Doctoral stay in the research group of Prof. T. Prisner with the Center for Biomolecular Magnetic Resonance, Goethe University, Frankfurt, Germany, he joined the research group of Prof. J. van Slageren with the University of Stuttgart, Stuttgart, Germany. In 2018, he established the MOTeS Group and became its Group Leader at CEITEC, BUT, Brno, Czech Republic. The group focuses on the development of high-frequency electron spin resonance (HF-ESR) spectroscopy, especially frequency rapid scan above 100 GHz (ERC grant), HF-ESR applications to molecular magnetism, thin films, and molecular materials.